International Journal of Heat and Mass Transfer 52 (2009) 3712–3725

Contents lists available at ScienceDirect

International Journal of Heat and Mass Transfer

journal homepage: www.elsevier.com/locate/ijhmt

Effective boundary conditions for rough reactive walls in laminar boundary layers

Stéphanie Veran, Yvan Aspa, Michel Quintard *

Université de Toulouse, INPT, UPS, IMFT (Institut de Mécanique des Fluides de Toulouse), Allée Camille Soula, F-31400 Toulouse, France
CNRS, IMFT, F-31400 Toulouse, France

ARTICLE INFO

Article history:
Received 11 September 2008
Received in revised form 11 January 2009
Accepted 20 January 2009
Available online 24 April 2009

Keywords:
Heterogeneous reactive surface
Domain decomposition
Closure problems
Effective surface

ABSTRACT

In order to gain computational time and simplicity, transfer over rough and heterogenous surfaces is most often modelled using the concept of an effective (flat) surface. In this paper, we are particularly interested in mass transport by convection and diffusion over rough, heterogeneous and reactive surfaces and we propose a model using first-order effective properties. The resolution of "*local closure problems*" given by a domain decomposition technique, allows to link flow and surface parameters to effective properties of the modelled fluid/solid interface: δ, the effective surface position, and k_{eff}, the effective reaction rate. The effect on δ and k_{eff} of the surface chemical and geometric properties, as well as the flow characteristics, is then analysed, giving some indications for possible estimates in specific cases. Finally, the obtained model is validated by comparison to direct numerical simulations.

1. Introduction

The problem of transport phenomena at the boundary between a free fluid and a complex interface can be found in many applications: chemical engineering, geochemistry, bioengineering with flow over biofilms to cite few examples. Numerous studies have been done on the case of turbulent boundary layers over rough surfaces since the early experiments of [1]. Since this origin, it was clear that the engineering practice would only require the knowledge of some average properties and not the flow in details at the roughness scale. This is also the case when one considers the problem of the interface between a fluid layer and a porous domain. This problem was studied for heat [2], mass [3] and momentum transfer [4–9]. Once again, it was found convenient for macro-scale modelling purposes to introduce an effective boundary condition.

In this paper, we consider the case of a laminar boundary layer over a rough, reactive surface. The phenomenology of the rough surface configuration and the one of the porous boundary configuration are very similar at the micro-scale (asperity or pore scale geometry). In the cases of laminar flows over rough or porous surfaces, the surface is the locus of an enhanced momentum loss compared to perfectly flat surfaces. For the considered laminar flows, this loss is mainly due to viscous effects whereas in the previous mentioned studies on turbulent cases the loss is caused by the asperity induced pressure drag. One of the motivations of this work was to improve the modelling of composite ablation in the aerospace context. Indeed, during ablation, the surface of the composite parts recedes. As this recession is not uniform, asperities appear at the composite surface. Previous works [10–12] have been done on the impact of mass diffusion on roughness on-set during ablation. In this study, the roughness is assumed to have reached a steady state for which the geometry in the moving reference frame does not evolve anymore.

As this study is only one of the first steps towards a realistic complete modelling of this phenomenon, the complexity of the physics has been reduced. Thus, for simplicity, the fluid is assumed to be viscous and incompressible and the system is isothermal. The problem studied here, illustrated by Fig. 1, is to compute the mass and momentum transfers over a rough surface Σ placed into a laminar boundary layer.

Direct numerical simulations (DNSs) of such systems are available approaches when the characteristic lengths of the macro-scale flow and the roughness have the same magnitude order: $l/L = O(1)$. When $l/L \ll 1$, direct simulations are not achievable anymore. In such cases, the behavior of the heterogeneities must be homogenized. The homogenization procedure aims at replacing the detailed properties of the surface by effective ones. These effective properties refer to a fictive wall, which, placed in the same conditions than the detailed heterogeneous one, shows the same macro-scale behavior. Effective properties are not simply a pure mathematical concept. For example, it is the effective reactivity of the surface which is measured experimentally when an experiment is driven at the L-scale.

The composite surface is the locus of an heterogeneous reaction between a gaseous reactant A of concentration c and the solid. This solid surface has a non-uniform reactivity. In the considered cases, the reactant is assumed to be diluted into the fluid in such a way that mass transfer has no direct impact on the momentum transfer. In addition to the previous considerations, the roughness are supposed to be small compared to the boundary layer thickness and

* Corresponding author. Tel.: +33 5 61 58 59 21; fax: +33 5 61 58 59 93.
E-mail address: michel.quintard@imft.fr (M. Quintard).

0017-9310/$ - see front matter © 2009 Elsevier Ltd. All rights reserved.
doi:10.1016/j.ijheatmasstransfer.2009.01.045

Nomenclature

Roman symbols

a	closure variable for the reactant concentration (dimensionless)
A_f	fiber reactive area (m^2)
A_m	matrix reactive area (m^2)
$A_{0,i}$	area of Σ_0 boundary (m^2)
A_Σ	total reactive area (m^2)
b	closure variable for the reactant concentration (m)
c	reactant concentration defined in Ω ($kg\,m^{-3}$)
$\widetilde{c_i}$	reactant concentration deviation in Ω_i ($kg\,m^{-3}$)
c_i	reactant concentration defined in Ω_i ($kg\,m^{-3}$)
C_0	reactant concentration defined in Ω_0 ($kg\,m^{-3}$)
d_r	distance between two consecutive asperities (m)
D	reactant diffusion coefficient ($m^2\,s^{-1}$)
Da	$= kl/D$, Damköhler number (dimensionless)
Da_f	fiber Damköhler number (dimensionless)
Da_m	matrix Damköhler number (dimensionless)
$\widehat{Da}$	mean Damköhler number over the surface Σ (dimensionless)
$\mathbf{e_1}$	unit normal vector linked to x (dimensionless)
$\mathbf{e_2}$	unit normal vector linked to y (dimensionless)
h_r	roughness height (m)
J	mass flux exchanged over the reactive surface ($kg\,s^{-1}$)
k	first-order reaction rate ($m\,s^{-1}$)
k^0_{eff}	effective reaction rate at $y = 0$ ($m\,s^{-1}$)
k^δ_{eff}	effective reaction rate at $y = w^0_x$ ($m\,s^{-1}$)
$\widehat{k}$	mean reaction rate over the surface ($m\,s^{-1}$)
k_f	fiber reaction rate ($m\,s^{-1}$)
k^0_{low}	k^0_{eff} estimate at low Da ($m\,s^{-1}$)
k^δ_{low}	k^δ_{eff} estimate at low Da ($m\,s^{-1}$)
k_m	matrix reaction rate ($m\,s^{-1}$)
l	characteristic length associated to the asperities (m)
l_i	Ω_i width (m)
L	characteristic length associated to Ω (m)
$\mathbf{n}$	unit normal vector on Σ pointing toward the fluid (dimensionless)
$\mathbf{n_{0,i}}$	unit normal vector on $\Sigma_{0,i}$ pointing toward the wall (dimensionless)
N	total mass of reactant in the global domain (kg)
p	pressure defined in Ω (Pa)
p_i	pressure defined in Ω_i (Pa)
$\tilde{p}_i$	pressure deviation defined in Ω_i (Pa)
P_0	pressure defined in Ω_0 (Pa)
Re	$= UL\rho/\mu$, global Reynolds number (dimensionless)
Re_l	$= \rho\tau_h l^2/\mu^2$, local Reynolds number (dimensionless)
r_k	reaction rate contrast (dimensionless)
Sc	$= \mu/\rho D$, Schmidt number (dimensionless)
$\mathbf{u}$	fluid velocity defined in Ω ($m\,s^{-1}$)
$\mathbf{u_i}$	fluid velocity defined in Ω_i ($m\,s^{-1}$)
$\tilde{\mathbf{u}}_\mathbf{i}$	fluid velocity deviation in Ω_i ($m\,s^{-1}$)
$\mathbf{U_0}$	fluid velocity defined in Ω_0 ($m\,s^{-1}$)
U	magnitude of $\mathbf{u}$ ($m\,s^{-1}$)
$\mathbf{w}$	closure variable for the fluid velocity in Ω_i (m)
w^0_x	distance between Σ_0 and Σ_{eff} (m)
x	abscissa (m)
y	ordinate (m)
y_N	effective surface position conserving N (m)

Greek symbols

δ	effective surface position (m)
δ^*	$= \delta/h_r$ (dimensionless)
λ	flow characteristic length (m)
μ	fluid dynamic viscosity (Pa s)
ν	fluid kinematic viscosity (m^2 s)
Ω	global domain (dimensionless)
ρ	fluid density ($kg\,m^{-3}$)
σ	stress (Pa)
Σ	rough reactive wall (dimensionless)
ϖ	closure variable for the pressure in Ω_i (Pa s)

the curvature of the surface is itself small compared to the asperities. As a first consequence, we expect some discrepancy between the developed model and actual results at the entrance region of the boundary layer. This question will be looked at in Section 5.

The boundary conditions that must be employed to build a direct simulation, i.e., small-scale description, over such a surface are well known. Therefore, without further considerations, we list below the small-scale problems to be solved. The problem for the momentum transfer is described by

$$\rho(\mathbf{u}.\nabla)\mathbf{u} - \mu\Delta\mathbf{u} + \nabla p = 0 \quad \text{in } \Omega, \tag{1}$$

$$\nabla\cdot\mathbf{u} = 0 \quad \text{in } \Omega, \tag{2}$$

$$\mathbf{u} = 0 \quad \text{on } \Sigma. \tag{3}$$

Let define Re the Reynolds number at the macro-scale by

$$Re = \frac{UL\rho}{\mu}, \tag{4}$$

where U is the magnitude of $\mathbf{u}$ and L is the flow macro-scale characteristic length.

The problem for mass transfer can be summarized as

$$\mathbf{u}\cdot\nabla c = \nabla\cdot D\nabla c \quad \text{in } \Omega, \tag{5}$$

$$-\mathbf{n}\cdot D\nabla c = kc \quad \text{on } \Sigma, \tag{6}$$

where k is a reaction rate that may depend on the position on the surface and $\mathbf{n}$ is the normal to Σ pointing from the fluid towards the solid. Eq. (6) is the boundary condition for mass transport for the case of a first-order irreversible reaction.

This paper intends to develop, in a unified formalism, the effective conditions for momentum and mass transfers over a rough, reactive, non-uniform surface. "Homogenization" techniques propose to link the observed macroscopic behavior to the micro-scale characteristics. The volume averaging approach [13] has been widely used in order to define the effective boundary conditions for a fluid-porous interface [6,5,7,14,15,9,3,8]. In these studies, the interfacial region is described at a mesoscopic scale where the solid and the fluid are replaced by a unique medium. The introduced medium is characterized by local properties (such as permeablility for instance) having smooth variations in the interfacial zone. The meso-scale properties are defined as being local spatial averages. By definition, the boundary is a singularity and this leads to some mathematical complexity when manipulating volume averages. While it is still possible to define spatial averages in this zone, the constraints of the classical "bulk" volume averaging approach cannot be satisfied in general. Nevertheless, the effective models obtained by the previously mentioned studies have shown a satisfying ability to describe the experimental data.

Effective boundary conditions for flat impermeable but non uniform reactive wall have been obtained by [16] using a volume averaging approach in the diffusive case. In order to extend this work to more complex interfaces, the idea is to split the whole domain into subdomains as it will be explained later on. This concept of domain decomposition was first introduced by [17] for the

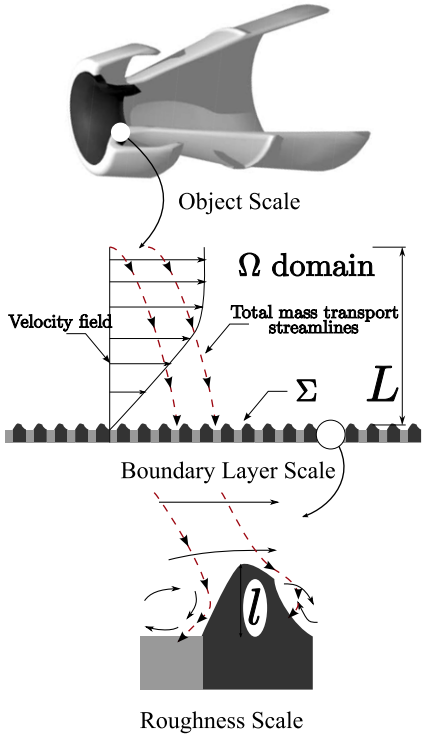

Fig. 1. Multiscale description of a laminar boundary layer over a reactive rough surface.

momentum transfer and it is extended in this paper for both momentum and mass transfer in a unified formalism. In the studied case, $l/L \ll 1$, the fluctuations of velocity and concentration introduced by the non-uniform wall are assumed to vanish far from the fluid/solid interface. Based on this assumption, a multidomain decomposition approach is conducted and an approximate solution is obtained which allows to build an effective surface with the associate effective boundary condition. These effective properties are explicitly linked to the surface structure and other fluid physical properties. In this paper, first-order effective properties are built. The effect of wall properties and transfer conditions on the obtained effective properties is then discussed. Finally, in order to validate the proposed models, numerical tests are presented in the last section of this article.

2. Multi-domain decomposition

In order to study a finite domain, we limit Ω by an upper surface Σ_e and by side surfaces Σ_l. The boundary conditions on these surfaces are assumed not to impact the homogenization procedure. Therefore, they will be given only in the application part. Of course, we already mentioned the possible breakdown of the major assumption made in this development, i.e., $l \ll L$, at some entrance regions. It will be shown in Section 5 that this does not impact the solution far beyond the entrance region, in our laminar case. In addition, the surface Σ is supposed to have a negligible curvature at the L-scale.

As mentioned before, the fluctuations of velocity and concentration vanish far from the wall and, at the L-scale these fields are smooth. This suggests a decomposition of the whole domain Ω into subdomains as illustrated by Fig. 2.

On the one hand, the domain Ω_0 (with $*_0$ quantities) corresponds to the restriction of Ω where the variables are smooth. On the other hand, the Ω_i (with $*_i$ quantities) domains contain all

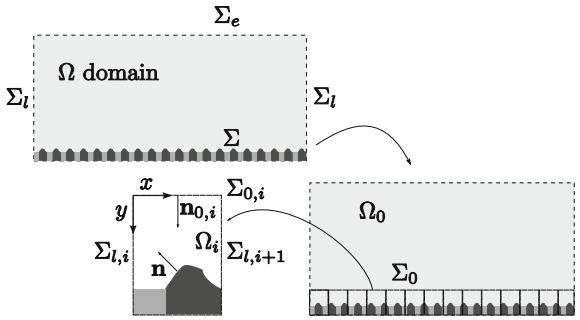

Fig. 2. Multi-domain decomposition.

the perturbation of the concentration and velocity fields. In the asymptotic method formalism, this is seen as being the matching of a function of a quickly varying variable in Ω_i domains with a function of a slowly varying variable in the Ω_0 domain. The direction $\mathbf{e}_1$ (x-coordinate) refers to the infinite flow direction. The direction $\mathbf{e}_2$ (y-coordinate) refers to the macroscopic wall normal. The third direction, $\mathbf{e}_3$, (z-coordinate) is transverse. If, as supposed, the asperities are z-periodic, the reactive flow problem is periodic in this direction and does not require any particular consideration. In this work, the theoretical developments are written in 3D. For practical reasons the numerical applications will be limited to 2D ($(\mathbf{e}_1, \mathbf{e}_2)$ plane).

Let name Σ_0 the boundary splitting Ω_0 from the Ω_i domains and $\Sigma_{0,i}$ the intersection of Σ_0 and $\partial\Omega_i$ (boundary of Ω_i). The surface dividing Ω_i from Ω_{i-1} is denoted $\Sigma_{l,i}$. The exact position of Σ_0 is not defined by an identified physical phenomenon. The choice of Σ_0 is nonetheless constrained by the fact that all the deviations due to the non-uniformity of Σ in terms of roughness and chemical reactivity must be contained in the Ω_i domains. This criterion is equivalent to a condition of minimum distance (unknown at this stage) between Σ and Σ_0. Because the damping of the deviation is smooth and the deviation is asymptotically tending towards zero, the definition of such a distance remains subjective. As Σ_0 is an arbitrary frontier in a continuous physical domain, the pressure, velocity and concentration must be continuous across Σ_0

$$\mathbf{U}_0 = \mathbf{u}_i \quad \text{on } \Sigma_{0,i}, \tag{7}$$
$$P_0 = p_i \quad \text{on } \Sigma_{0,i}, \tag{8}$$
$$C_0 = c_i \quad \text{on } \Sigma_{0,i}. \tag{9}$$

For the same reasons, the mass flux and the stress must also be continuous. The stress continuity writes

$$\mathbf{n}_{0,i} \cdot \boldsymbol{\sigma}(\mathbf{U}_0) = \mathbf{n}_{0,i} \cdot \boldsymbol{\sigma}(\mathbf{u}_i) \quad \text{on } \Sigma_{0,i} \tag{10}$$

with the stress tensor $\sigma(\mathbf{u}) = p\mathbf{I} + \mu(\nabla\mathbf{u} + \nabla\mathbf{u}^T)$. The continuity of pressure leads to the following simplified expression for the stress continuity:

$$\mathbf{n}_{0,i} \cdot (\nabla\mathbf{U}_0 + \nabla\mathbf{U}_0^T) = \mathbf{n}_{0,i} \cdot (\nabla\mathbf{u}_i + \nabla\mathbf{u}_i^T) \quad \text{on } \Sigma_{0,i}. \tag{11}$$

The problems for the momentum and mass transfer in Ω_0 can be written as follows as being a spatial restriction of the problems in Ω completed by the continuity conditions:

Pb $\mathbf{I}_u$ (in Ω_0):

$$\rho(\mathbf{U}_0.\nabla)\mathbf{U}_0 - \mu\Delta\mathbf{U}_0 + \nabla P_0 = 0 \quad \text{in } \Omega_0, \tag{12}$$
$$\nabla \cdot \mathbf{U}_0 = 0 \quad \text{in } \Omega_0, \tag{13}$$
$$\mathbf{n}_{0,i} \cdot (\nabla\mathbf{U}_0 + \nabla\mathbf{U}_0^T) = \mathbf{n}_{0,i} \cdot (\nabla\mathbf{u}_i + \nabla\mathbf{u}_i^T) \quad \text{on } \Sigma_{0,i}, \tag{14}$$
$$\mathbf{U}_0 = \mathbf{u}_i \quad \text{on } \Sigma_{0,i}, \tag{15}$$
$$P_0 = p_i \quad \text{on } \Sigma_{0,i}. \tag{16}$$

Pb $\mathbf{I}_c$ (in Ω_0):

$$\mathbf{U}_0\cdot\nabla C_0=\nabla\cdot(D\nabla C_0)\ \text{ in }\Omega_0, \tag{17}$$

$$-\mathbf{n}\cdot D\nabla C_0=0\ \text{ on }\Sigma_l, \tag{18}$$

$$\int_{\Sigma_{0,i}}\mathbf{n}_{0,i}\cdot(-D\nabla C_0+\mathbf{U}_0C_0)dA = \int_{\Sigma_{0,i}}\mathbf{n}_{0,i}\cdot(-D\nabla c_i+\mathbf{U}_0c_i)dA\ \text{ on }\Sigma_{0,i}, \tag{19}$$

$$C_0=c_i\ \text{ on }\Sigma_{0,i}, \tag{20}$$

in which $\mathbf{n_{0,i}}$ is the normal vector to $\Sigma_{0,i}$ pointing from the Ω_0 domain towards Ω_i cell.

In the different Ω_i domains, the boundary conditions given by Eqs. (14), (15), (19) and (20) must remain unchanged. The conservation equations for the variables take the same form as in Ω. Moreover, the fields are supposed to be pseudo-periodic at the l-scale. This is equivalent to assume the transverse fluxes (crossing $\Sigma_{l,i}$) to be negligible compared to the fluxes coming from $\Sigma_{0,i}$. These assumptions lead to the following problems:

Pb $\mathbf{II}_u$ (in Ω_i):

$$\rho(\mathbf{u}_i\cdot\nabla)\mathbf{u}_i-\mu\Delta\mathbf{u}_i+\nabla p_i=0\quad\text{in }\Omega_i, \tag{21}$$

$$\nabla\cdot\mathbf{u}_i=0\quad\text{in }\Omega_i, \tag{22}$$

$$\mathbf{u}_i=0\quad\text{on }\Sigma, \tag{23}$$

$$\mathbf{u}_i(x+l_i)=\mathbf{u}_i(x)\quad\text{on }\Sigma_l, \tag{24}$$

$$p_i(x+l_i)=p_i(x)\quad\text{on }\Sigma_l, \tag{25}$$

$$\mathbf{n}_{0,i}\cdot(\nabla\mathbf{U}_0+\nabla\mathbf{U}_0^T)=\mathbf{n}_{0,i}\cdot(\nabla\mathbf{u}_i+\nabla\mathbf{u}_i^T)\quad\text{on }\Sigma_{0,i}, \tag{26}$$

$$\mathbf{u}_i=\mathbf{U}_0\quad\text{at }\Sigma_{0,i}, \tag{27}$$

$$p_i=P_0\quad\text{on }\Sigma_{0,i}. \tag{28}$$

Pb $\mathbf{II}_c$ (in Ω_i):

$$\mathbf{u}_i\cdot\nabla c_i=\nabla\cdot(D\nabla c_i)\quad\text{in }\Omega_i, \tag{29}$$

$$-\mathbf{n}\cdot D\nabla c_i=kc_i\quad\text{on }\Sigma, \tag{30}$$

$$c_i(x+l_i)=c_i(x)\quad\text{on }\Sigma_l, \tag{31}$$

$$\int_{\Sigma_{0,i}}\mathbf{n}_{0,i}\cdot(-D\nabla C_0+\mathbf{u}_iC_0)dA = \int_{\Sigma_{0,i}}\mathbf{n}_{0,i}\cdot(-D\nabla c_i+\mathbf{u}_ic_i)dA\quad\text{on }\Sigma_{0,i}C_0=c_i\ \text{ at }\Sigma_{0,i}. \tag{32}$$

At this stage, the problems allowing to compute the velocity and concentration field in the two domains are obtained. One can choose to solve numerically the problems in the Ω_i domains as written above. Nevertheless, if this computation is done in every Ω_i domain and is coupled to the computation of the problem in Ω_0, the decomposition approach leads to limited or zero gain in the computational cost. To obtain a significant reduction of the computational cost, one can try to build a generic solution on the Ω_i domains and replace the computing between Ω_i and Ω_0 by an effective boundary condition.

A greater reduction of the computational cost can be obtained by finding estimates of $\mathbf{u}_i$, p_i and c_i and then by obtaining a "*closed form*" for the boundary conditions involving $\mathbf{U}_0, P_0, C_0$ and their derivatives. In this paper, a so called first-order estimate is built and then compared to direct numerical simulations.

3. First-order effective laws

Wall laws for laminar flows given by asymptotic techniques have been determined by Achdou et al. in diverse studies [17] (steady incompressible Navier–Stokes flows), [18] (unsteady incompressible Navier–Stokes flows). Jäger, Devigne and Mikelić also worked on similar wall laws giving detailed mathematical proofs [19–21]. In [17], zero-, first- and second-order laws were defined to model flows over periodic rough surfaces. Using their works as a basis, a different implementation of the effective surface for momentum transfer is developed. The main difference appears when the effective position of the surface is chosen and defined as it will be detailed later.

In this section, estimates for the local fields of velocity, pressure and concentration, respectively $\mathbf{u}_i$, p_i and c_i are built. Using the closed form of the problems in Ω_0, one shows that effective surfaces can be built both for momentum and mass transfer. The effective condition aims at replacing the real surface Σ by a simpler flat one over which effective boundary conditions are applied in order to reproduce the behavior of the detailed system.

3.1. Momentum boundary condition

Let define $\tilde{\mathbf{u}}_i$ the deviation of the velocity in the Ω_i domain by the difference between the local velocity field $\mathbf{u}_i$ and the global field $\mathbf{u}$:

$$\mathbf{u}_i=\mathbf{u}+\tilde{\mathbf{u}}_i. \tag{33}$$

This global velocity field $\mathbf{u}$, can be defined in Ω_0 as $\mathbf{U}_0$ and in Ω_i as being an expansion of $\mathbf{U}_0$ under the form of a Taylor development. Under this consideration and neglecting variations of $\mathbf{U}_0$ and P_0 along $\Sigma_{0,i}$, Eq. (33) becomes

$$\mathbf{u}_i=\underbrace{\mathbf{U}_0|_{y=0}+\mathbf{y}\cdot\nabla\mathbf{U}_0|_{y=0}+\frac{1}{2}\mathbf{y}\mathbf{y}\cdot\nabla\nabla\mathbf{U}_0|_{y=0}+\cdots}_{u}+\tilde{\mathbf{u}}_i. \tag{34}$$

It is interesting to notice here that the decomposition given by Eq. (34) is reminiscent of the strategy proposed by the different authors, i.e., as a decomposition in terms of smooth macro-scale field and a fluctuation. The field $\mathbf{u}$ plays the role of the mesoscopic field introduced in [5]. Nevertheless, in our approach this expansion of the macroscopic field has a clear mathematical definition and we do not assume here that this function represents a physical variable coming from some averaging process.

Using this definition of $\tilde{\mathbf{u}}_i$, Eq. (3) implies that in terms of magnitude

$$\tilde{\mathbf{u}}_i=O(\mathbf{u}_i)=O\left(\frac{l}{L}U\right) \tag{35}$$

with U the magnitude of $\mathbf{u}$. Injecting the definition of the deviation $\tilde{\mathbf{u}}_i$, Eq. (33), into Eq. (21) gives at first order the following relation:

$$0=\underbrace{(\mathbf{u}\cdot\nabla)\mathbf{u}-\nu\Delta\mathbf{u}+\rho^{-1}\nabla p}_{=0}+\underbrace{(\mathbf{u}\cdot\nabla)\tilde{\mathbf{u}}_i}_{o\left(\frac{U^2}{L}\right)} +\underbrace{(\tilde{\mathbf{u}}_i\cdot\nabla)\mathbf{u}}_{o\left(\frac{U^2}{L}\right)}+\underbrace{(\tilde{\mathbf{u}}_i\cdot\nabla)\tilde{\mathbf{u}}_i}_{o\left(\frac{U^2l}{L^2}\right)}-\underbrace{\nu\Delta\tilde{\mathbf{u}}_i}_{o\left(\frac{U^2}{LRe}\right)}+\rho^{-1}\nabla\tilde{p}_i, \tag{36}$$

where $\tilde{p}_i$ is the deviation of the pressure defined by analogy with $\tilde{\mathbf{u}}_i$.

As said before, the considered roughness is small compared to the boundary layer thickness. This assumption leads to $(1/Re)\gg(l/L)$. Therefore, Eq. (36) reduces to

$$-\mu\Delta\tilde{\mathbf{u}}_i+\nabla\tilde{p}_i=0. \tag{37}$$

By using the difference between Eqs. (22) and (2), one finally obtains

$$\nabla\cdot\tilde{\mathbf{u}}_i=0. \tag{38}$$

Below, we look for the problem defining $\mathbf{u}_i$ at first order, i.e., keeping in the development of $\mathbf{u}$ in Eq. (34) the terms involving $\mathbf{U}_0|_{y=0}$ and $\nabla\cdot\mathbf{U}_0|_{y=0}$.

$$\mathbf{u}_i=\mathbf{U}_0|_{y=0}+\mathbf{y}\cdot\nabla\mathbf{U}_0|_{y=0}+\tilde{\mathbf{u}}_i. \tag{39}$$

There we see that the assumption $l\ll L$ is crucial for the quality of this approximation.

In the studied configuration, the free fluid region represents a boundary layer. As a consequence, the normal variations close to the wall are greater than the tangential ones ($\partial_y \gg \partial_x, \partial_z$). Moreover, the velocity is mainly tangential and first-order terms in Eq. (34) can be simplified to

$$\mathbf{y}\cdot\nabla\mathbf{U}_0|_{y=0} = y\frac{\partial U_0}{\partial y}\bigg|_{y=0}\mathbf{e}_1. \tag{40}$$

For the same reasons, the stress continuity on $\Sigma_{0,i}$ simplifies to the continuity of the shear stress given by

$$\mathbf{n}_{0,i}\cdot\frac{\partial\mathbf{U}_0}{\partial y} = \mathbf{n}_{0,i}\cdot\frac{\partial\mathbf{u}_i}{\partial y} \quad \text{on } \Sigma_{0,i}. \tag{41}$$

From Eq. (23), the boundary condition on Σ is obtained as

$$U_0|_{y=0}\mathbf{e}_1 + y\frac{\partial U_0}{\partial y}\bigg|_{y=0}\mathbf{e}_1 + \tilde{\mathbf{u}}_i = 0 \quad \text{on } \Sigma. \tag{42}$$

An intermediate variable λ having the dimension of a length, is introduced by the following definition:

$$\lambda = -\frac{U_0}{\frac{\partial U_0}{\partial y}\Big|_{y=0}}. \tag{43}$$

As written before, the curvature of Σ_0 is negligible. The normal to Σ_0 is simply $\mathbf{n}_{0,i} = \mathbf{e}_2$. The momentum flux continuity on Σ_0 given by Eq. (41) is rewritten as

$$\frac{\partial\mathbf{u}_i}{\partial y} = \frac{\partial U_0}{\partial y}\mathbf{e_1} \quad \text{on } \Sigma_0. \tag{44}$$

For the left-hand side, the use of the decomposition given by Eq. (34) with the assumption of boundary layer flow, leads to

$$\frac{\partial\mathbf{u}_i}{\partial y} = \frac{\partial U_0}{\partial y}\bigg|_{y=0}\mathbf{e}_1 + \frac{\partial\tilde{\mathbf{u}}_i}{\partial y}. \tag{45}$$

Collecting the obtained equations and adding the periodic constraints on the deviations, which are justified if the considered $\Omega_{0,i}$ domain is far enough from the beginning of the boundary layer, the problem for the deviations may be summarized by **Pb II**$_{\tilde{u}}$ (in Ω_i):

$$-\mu\Delta\tilde{\mathbf{u}}_i + \nabla\tilde{p}_i = 0 \quad \text{in } \Omega_i, \tag{46}$$

$$\nabla\cdot\tilde{\mathbf{u}}_i = 0 \quad \text{in } \Omega_i, \tag{47}$$

$$(\lambda + y)\frac{\partial U_0}{\partial y}\bigg|_{y=0}\mathbf{e}_1 + \tilde{\mathbf{u}}_i = 0 \quad \text{on } \Sigma, \tag{48}$$

$$\frac{\partial\tilde{\mathbf{u}}_i}{\partial y} = \mathbf{0} \quad \text{on } \Sigma_{0,i}, \tag{49}$$

$$\tilde{p}_i = 0 \quad \text{on } \Sigma_{0,i}, \tag{50}$$

$$\tilde{\mathbf{u}}_i(x + l_i) = \tilde{\mathbf{u}}_i(x) \quad \text{on } \Sigma_l, \tag{51}$$

$$\tilde{p}_i(x + l_i) = \tilde{p}_i(x) \quad \text{on } \Sigma_l, \tag{52}$$

in which l_i is the Ω_i domain length. At this stage, the problem must be closed by linking the deviation to the macro-scale behavior. This is done by seeking the solutions under the following form:

$$\tilde{\mathbf{u}}_i = (\mathbf{w} - \lambda\mathbf{e}_1)\frac{\partial U_0}{\partial y}\bigg|_{y=0}, \tag{53}$$

$$\tilde{p}_i = \varpi\frac{\partial U_0}{\partial y}\bigg|_{y=0}. \tag{54}$$

One obtains the following problem for the closure variables $\mathbf{w}$ and ϖ:**Pb II**$_w$ (in Ω_i):

$$-\mu\Delta\mathbf{w} + \nabla\varpi = 0 \quad \text{in } \Omega_i, \tag{55}$$

$$\nabla\cdot\mathbf{w} = 0 \quad \text{in } \Omega_i, \tag{56}$$

$$\mathbf{w} = -y\mathbf{e}_1 \quad \text{on } \Sigma, \tag{57}$$

$$\frac{\partial\mathbf{w}}{\partial y} = \mathbf{0} \quad \text{on } \Sigma_{0,i}, \tag{58}$$

$$\varpi = 0 \quad \text{on } \Sigma_{0,i}, \tag{59}$$

$$\mathbf{w}(x + l_i) = \mathbf{w}(x) \quad \text{on } \Sigma_l, \tag{60}$$

$$\varpi(x + l_i) = \varpi(x) \quad \text{on } \Sigma_l. \tag{61}$$

A closed formulation of the problem **Pb I**$_u$ can now be built using the velocity continuity at Σ_0 (Eq. (15)). This equation implies that the deviation $\tilde{\mathbf{u}}_i$ is zero on Σ_0. Using this condition and the closure equation Eq. (53), one simply has $\mathbf{w}|_{y=0} = \lambda\mathbf{e}_1$. Introducing the notation $w_x^0 = \mathbf{w}|_{y=0}\cdot\mathbf{e}_1$, we may write this last equation under the form of a closed expression for the macro-scale field and its derivatives, i.e., an effective boundary condition. We have

$$\mathbf{U}_0 = -w_x^0\frac{\partial U_0}{\partial y}\mathbf{e}_1 \quad \text{on } \Sigma_0. \tag{62}$$

One must note that this effective boundary condition is similar to the one obtained at first order in [22]. The problem for the macro-scale flow U_0 has been closed with a boundary condition on Σ_0. At first order, the Taylor development of the macro-scale velocity U_0 at $y = w_x^0$ gives

$$U_0(w_x^0) = U_0|_{y=0} + w_x^0\frac{\partial U_0}{\partial y}\bigg|_{y=0}. \tag{63}$$

Using Eq. (62) in this development shows that the length w_x^0 represents the distance between Σ_0 and a fictive surface Σ_{eff} parallel to Σ_0 where the boundary condition becomes

$$\mathbf{U}_0 = \mathbf{0} \quad \text{on } \Sigma_{\mathbf{eff}}. \tag{64}$$

This configuration is illustrated in Fig. 3. As explained before, the position of Σ_0 is somehow arbitrary and, as a consequence, the obtained value for the length w_x^0 is not an intrinsic physical parameter of the problem. For example, in the asymptotic limit of a flat surface for Σ, w_x^0 would be equal to the distance between Σ and Σ_0. In order to build a more meaningful distance, it is more convenient to define δ as being the distance between the lower part of Σ and Σ_{eff}. In addition, the no-slip boundary condition, associated to Σ_{eff}, is easier to apply than a wall law where the velocity boundary condition on the effective surface depends on its derivatives (as it is done in the work of Achdou et al., e.g., [17]).

One can note that in **Pb II**$_w$ the viscosity μ only acts as a scaling of the pressure deviation ϖ. As a result, the $\mathbf{w}$ field depends only on the roughness geometry and not on the flow properties. Thus, for the previously considered system and for a periodic rough surface, the effective length δ will be uniform and independent of the local Reynolds number.

At this step, the procedure for the momentum transfer can be summarized as follow:

(1) The global domain Ω is divided into a macro-scale subdomain Ω_0 and a collection of micro-scale subdomains Ω_i.
(2) An estimation of the momentum transfer in the Ω_i domains is built as being the sum of an asymptotic expansion of the macro-scale flow and a deviation term.
(3) The deviation has been linked to the macro-scale flow using closure variables.

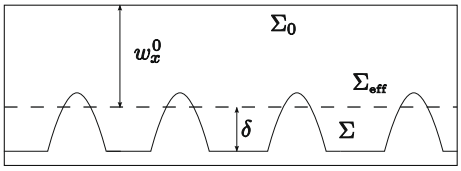

Fig. 3. Definition of the effective surface Σ_{eff}.

(4) The solving of the closure problem leads to the definition of an effective surface Σ_{eff} (its position) and the effective boundary conditions.
(5) The closed problem for the momentum transfer at the macro-scale can be written now as

$$\rho(\mathbf{U}_0\cdot\nabla)\mathbf{U}_0-\mu\Delta\mathbf{U}_0+\nabla P_0=0 \quad \text{in } \Omega_0, \tag{65}$$
$$\nabla\cdot\mathbf{U}_0=0 \ \text{ in } \Omega_0, \tag{66}$$
$$\mathbf{U}_0=\mathbf{0} \quad \text{on } \Sigma_{\text{eff}}. \tag{67}$$

Here our choice of Σ_{eff} as the effective surface implies Eq. (67). We remind the reader that other choices are possible that may result in a Navier-like wall law.

In the next section, this method will be used once more in order to obtain an effective surface and boundary condition for the mass transfer problem.

3.2. Mass boundary condition

In **Pb II**$_c$, the velocity in the Ω_i domains is $\mathbf{u}_i$. The previous section showed how estimates for the velocity could be built. Therefore, as momentum and mass transfers can be uncoupled, it is chosen to write the mass transfer equations in Ω_i using the global velocity $\mathbf{u}$.

In this part, the previous procedure is used to obtain the effective boundary conditions for mass transfer. Under the same assumptions than for the momentum "homogenization", one tries to find an approximated solution of the problem by introducing the following estimate for c_i:

$$c_i=C_0|_{y=0}+y\left.\frac{\partial C_0}{\partial y}\right|_{y=0}+\tilde{c}_i. \tag{68}$$

As a consequence, the different equations in **Pb II**$_c$ can be rewritten as follows. Eq. (29) becomes

$$v\left.\frac{\partial C_0}{\partial y}\right|_{y=0}+\mathbf{u}\cdot\nabla\tilde{c}_i=\nabla\cdot(D\nabla\tilde{c}_i) \tag{69}$$

and Eq. (30)

$$-\mathbf{n}\cdot\left(D\left.\frac{\partial C_0}{\partial y}\right|_{y=0}\mathbf{e_2}\right)-\mathbf{n}\cdot D\nabla\tilde{c}_i=k\left(C_0|_{y=0}+y\left.\frac{\partial C_0}{\partial y}\right|_{y=0}+\tilde{c}_i\right) \quad \text{on } \Sigma, \tag{70}$$

in which $\tilde{c}_i$ is the concentration deviation term similarly defined as for the velocity, Eq. (68).

Adding the continuity condition across $\Sigma_{0,i}$ and the periodicity constraint, the problem for $\tilde{c}_i$ becomes

Pb II$_{\tilde{c}}$ (in Ω_i):

$$v\left.\frac{\partial C_0}{\partial y}\right|_{y=0}+\mathbf{u}\cdot\nabla\tilde{c}_i=\nabla\cdot(D\nabla\tilde{c}_i) \quad \text{in } \Omega_i, \tag{71}$$
$$\tilde{c}_i(x+l_i)=\tilde{c}_i(x) \quad \text{on } \Sigma_l, \tag{72}$$
$$\tilde{c}_i=0 \quad \text{on } \Sigma_{0,i}, \tag{73}$$
$$-\mathbf{n}\cdot\left(D\left.\frac{\partial C_0}{\partial y}\right|_{y=0}\mathbf{e_2}\right)-\mathbf{n}\cdot D\nabla\tilde{c}_i= \tag{74}$$
$$k\left(C_0|_{y=0}+y\left.\frac{\partial C_0}{\partial y}\right|_{y=0}+\tilde{c}_i\right) \quad \text{on } \Sigma. \tag{75}$$

Given the properties of this system, one can seek a solution of this problem in terms of

$$\tilde{c}_i=aC_0|_{y=0}+b\left.\frac{\partial C_0}{\partial y}\right|_{y=0}, \tag{76}$$

where a and b are first-order mapping variables.

We have from Eq. (75)

$$-\mathbf{n}\cdot D\left.\frac{\partial C_0}{\partial y}\right|_{y=0}(\mathbf{e_2}+\nabla b)-\mathbf{n}\cdot DC_0|_{y=0}\nabla a = k\left(C_0|_{y=0}(1+a)+(b+y)\left.\frac{\partial C_0}{\partial y}\right|_{y=0}\right) \tag{77}$$

and **Pb II**$_{\tilde{c}}$ may be transformed in two independent problems for a and b. We have

Pb II$_a$ (in Ω_i):

$$\mathbf{u}\cdot\nabla a=\nabla\cdot(D\nabla a), \tag{78}$$
$$a(x+l_i)=a(x) \ \text{ on } \Sigma_l, \tag{79}$$
$$a=0 \ \text{ on } \Sigma_{0,i}, \tag{80}$$
$$-\mathbf{n}\cdot D\nabla a=k(1+a) \quad \text{on } \Sigma. \tag{81}$$

Pb II$_b$ (in Ω_i):

$$v+\mathbf{u}\cdot\nabla b=\nabla\cdot(D\nabla b), \tag{82}$$
$$b(x+l_i)=b(x) \quad \text{on } \Sigma_l, \tag{83}$$
$$b=0 \quad \text{on } \Sigma_{0,i}, \tag{84}$$
$$-D\mathbf{n}\cdot\mathbf{e}_2-\mathbf{n}\cdot D\nabla b=k(y+b) \quad \text{on } \Sigma. \tag{85}$$

At this point, one can note that $b=-y$ is solution of this previous system of equations. As a result, c_i is simplified as

$$c_i=(1+a)C_0|_{y=0}. \tag{86}$$

We are now in a position to use Eq. (19) to determine the boundary condition at $\Sigma_{0,i}$ which gives a closed form of **Pb I**$_c$. We have

$$\int_{\Sigma_{0,i}}\mathbf{n}_{0,i}\cdot(-D\nabla C_0+\mathbf{u}C_0)dA=\int_{\Sigma_{0,i}}\mathbf{n}_{0,i}\cdot(-D\nabla c_i+\mathbf{u}c_i)dA \quad \text{at } \Sigma_{0,i}. \tag{87}$$

As the continuity of the concentration on $\Sigma_{0,i}$ gives $c_i=C_0$. The previous equation simplifies to

$$\int_{\Sigma_{0,i}}\mathbf{n}_{0,i}\cdot D\nabla C_0\,dA=\int_{\Sigma_{0,i}}\mathbf{n}_{0,i}\cdot D\nabla c_i\,dA \quad \text{at } \Sigma_{0,i} \tag{88}$$

with $\mathbf{n}_{0,i}=\mathbf{e_2}$:

$$D\left.\frac{\partial C_0}{\partial y}\right|_{y=0}=\frac{C_0|_{y=0}D}{A_{0,i}}\int_{\Sigma_{0,i}}\frac{\partial a}{\partial y}dA. \tag{89}$$

As mentioned before, the transverse mass fluxes are neglected compared to the vertical ones. This assumption leads to the pseudo-periodicity of the concentration fields at the l-scale. Thus, the flux balance on Ω_i becomes

$$\int_{\Sigma_{0,i}}\mathbf{n}_{0i}\cdot D\nabla a\,dA=\int_{\Sigma}\mathbf{n}\cdot D\nabla a\,dA. \tag{90}$$

Eq. (90) can be transformed using Eq. (81):

$$-\int_{\Sigma_{0,i}}\mathbf{n}_{0i}\cdot D\nabla a\,dA=-\int_{\Sigma}\mathbf{n}\cdot D\nabla a\,dA=\int_{\Sigma}k(1+a)dA. \tag{91}$$

Finally, the problem **Pb I**$_c$ may be written at first order in the following closed form:

$$\mathbf{u}\cdot\nabla C_0=\nabla\cdot(D\nabla C_0), \tag{92}$$
$$-\mathbf{n}\cdot D\nabla C_0=0 \quad \text{at } \Sigma_l, \tag{93}$$
$$D\left.\frac{\partial C_0}{\partial y}\right|_{y=0}=\frac{-C_0|_{y=0}}{A_{0,i}}\int_{\Sigma}k(1+a)dA \quad \text{on } \Sigma_0. \tag{94}$$

As it was done in the previous section, imposing a condition in Σ_0 is not fully satisfactory because of its arbitrary position. An effective surface for momentum transfer called Σ_{eff}, was defined before

as being the surface at which the macro-scale problem is characterized by a no-slip condition. While other choices are available, we think it is convenient to move the lower boundary condition for mass transfer to this surface. This solution leads to have the boundary conditions for mass and momentum transfer applied on the same unique surface, which is obviously easier for routine application of this approach, in particular for numerical modelling. At first order, the macro-scale concentration on Σ_{eff} is (remember that it has been found that w_x^0 is the distance between Σ_0 and Σ_{eff})

$$C_0|_{y=w_x^0} = C_0|_{y=0} + w_x^0 \left.\frac{\partial C_0}{\partial y}\right|_{y=0}. \tag{95}$$

As $\partial C_0/\partial y$ is not y-dependent, Eq. (94) rewrites

$$D\left.\frac{\partial C_0}{\partial y}\right|_{y=w_x^0} = -\left(C_0|_{y=w_x^0} - w_x^0 \left.\frac{\partial C_0}{\partial y}\right|_{y=w_x^0}\right) k_{\text{eff}}^0, \tag{96}$$

where $k_{\text{eff}}^0 = \frac{1}{A_{0,i}} \int_\Sigma k(1+a)dA$.

Finally, let introduce k_{eff}^δ, the *effective reaction coefficient relative to* Σ_{eff} equal to

$$k_{\text{eff}}^\delta = \frac{k_{\text{eff}}^0}{1 - \frac{w_x^0}{D} k_{\text{eff}}^0}. \tag{97}$$

This expression shows that k_{eff}^δ depends on the position of Σ_{eff} through w_x^0, but not on the position of Σ_0, as k_{eff}^0 varies with the position of Σ_0. Using the fact that $\mathbf{n} = \mathbf{e_2}$, the boundary condition on Σ_{eff} finally writes

$$-\mathbf{n} \cdot D\nabla C_0 = k_{\text{eff}}^\delta C_0 \quad \text{on } \Sigma_{\text{eff}}. \tag{98}$$

A closed smoothed form of the mass and the momentum transfer over a rough reactive surface has been obtained. For practical implementation of the homogenized problem, it has been chosen to move the boundary conditions on a same surface for both problems. With such a choice, the obtained smoothed problem takes the form of a micro-scale problem. For this reason, the implementation of the macro-scale problem can be easily spread on commercial codes and used in industrial context.

The effective boundary conditions were built in order to obtain the average behavior of the studied variables. Therefore, there is no reason that the effective surface Σ_{eff} defined by the momentum transfer problem satisfies the conservation of the total "mass" $\int_\Omega c dV$. In the last part of this article, this error will be estimated numerically. It will be shown that the mass loss is reasonably acceptable and can be neglected. Details on the mass loss determination can be found in Appendix A. If the mass loss becomes a problem for a particular application, it is possible to use another definition of the effective surface position for the mass transfer problem that will satisfy this condition. The effective boundary condition will therefore change its value following Eq. (95) through (98). Another possibility, which could prove interesting if transient phenomena become important, is to adopt a new point of view, with the introduction of an excess surface concentration. Nevertheless, the development of such a model is beyond the scope of this paper.

Finally, the homogenization technique for the mass transfer problem can be summarized by the following steps:

(1) Similarly to the procedure for momentum transfer:
   - The domain Ω is decomposed in Ω_0 and Ω_i domains.
   - An estimate of the concentration is built in the Ω_i domains, as being the sum of an asymptotic expansion of the macro-scale concentration and a deviation term.
   - The deviation is linked to the macro-scale concentration using closure variables.

(2) The solving of the closure problem leads to the definition of an effective reaction rate, k_{eff}^0 at Σ_0.

(3) In order to link the two modellings (momentum and mass), the effective surface is chosen to be unique. In order to keep the no-slip condition for the flow problem, a new effective reaction rate is defined over Σ_{eff}: k_{eff}^δ.

(4) The closed problem for the mass transfer at the macro-scale is then written

$$\mathbf{u} \cdot \nabla C_0 = \nabla \cdot (D\nabla C_0), \tag{99}$$

$$-\mathbf{n} \cdot D\nabla C_0 = 0 \quad \text{at } \Sigma_l, \tag{100}$$

$$-\mathbf{n} \cdot D\nabla C_0 = k_{\text{eff}}^\delta C_0 \quad \text{on } \Sigma_{\text{eff}}. \tag{101}$$

4. Effective boundary conditions: numerical results

In the previous section, we have introduced two macro-scale models using the concept of an effective surface. The position, δ, and effective boundary conditions have been derived from the domain decomposition idea, in particular an effective reaction rate has been obtained, k_{eff}. The purpose of this section is to analyse the impact of the different parameters, such as surface geometry and chemical characteristics, or flow properties, on these effective values. Parametric numerical simulations are conducted over elementary cells to solve **Pb II**$_w$ and **Pb II**$_a$. Results of this study are the following.

4.1. Effective position of the surface

The geometry of the asperities and their density over the surface have a great impact on the position of the effective surface, δ. An interesting parameter is the ratio between δ and the roughness height, that we will call δ^*. Its evolution in function of the roughness shape, the roughness density and height is studied. Results of numerical simulations conducted for **Pb II**$_w$ in different elementary cells are summarized in the following figures from Figs. 4–7. First, three symmetrical roughness geometries are studied: cones, semi-ellipses and rectangles. In Fig. 5, δ^* is given for different distances between two consecutive asperities, d_r, and height, h_r. The surface geometries are illustrated in Fig. 4.

Parameter δ^* controls the ability of the fluid to flow between consecutive asperities. When the roughness density is high (i.e., distance between roughness is small), the fluid has difficulties to flow between asperities. As a consequence, the position of the effective surface will be nearly equal to the roughness height. This is illustrated in Fig. 5, which shows that δ^* is close to one for low d_r.

On the same figure, one can see that a steeper asperity opposes more resistance to the flow. For example, with identical h_r and d_r, changing the roughness shape from a triangular one to a rectangular one increase the steepness as well as the value of δ^*. Furthermore, for unchanged shape and d_r, δ^* also increases with h_r.

On the opposite, when d_r increases, the flow meets lower resistance. As a result, δ^* decreases and will tend to zero for large values

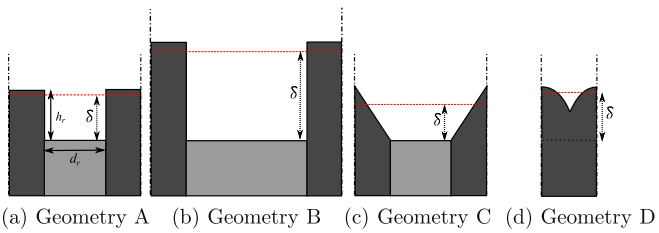

Fig. 4. Examples of cells used to obtain results shown in Fig. 5.

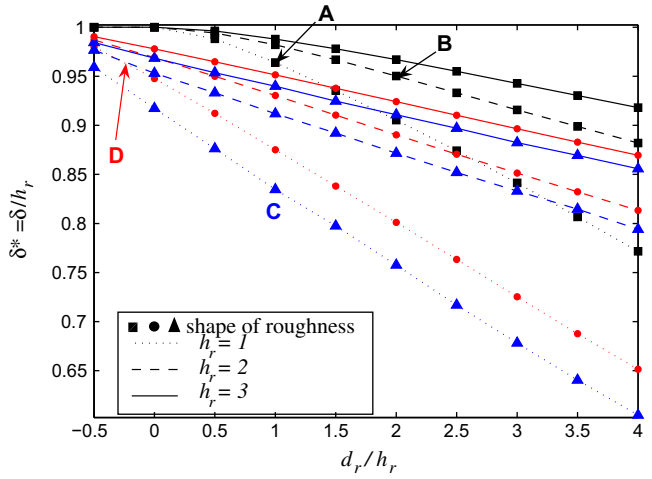

Fig. 5. Effective surface position for different roughness types, height and density. Square symbols correspond to rectangular roughness type, circle to ellipsoidal one and triangle to conic one, as illustrated in Fig. 4.

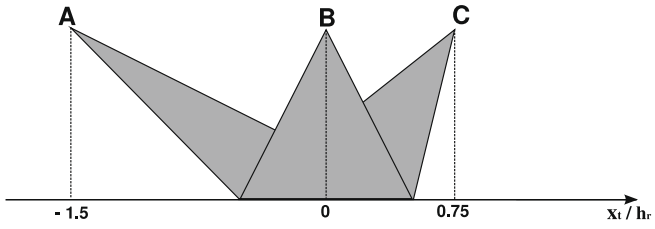

Fig. 6. Examples of triangular shapes used to obtain results shown in Fig. 7.

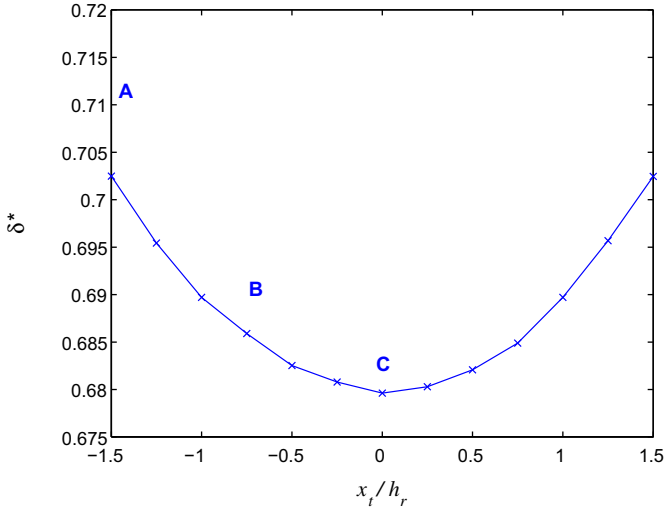

Fig. 7. Effective surface position for different triangular shapes.

of d_r. In this particular case, one asperity is far enough from its previous neighbour to see an unperturbed upstream flow.

Dissymmetrical surface geometries give similar results. Fig. 7 represents the variation of δ^* in function of the triangle top abscissa, x_t, as shown in Fig. 6. It shows that steeper asperities give higher positions of the effective surface. It is important to note that, as **Pb II**$_w$ is symmetrical with x, the evolution of δ^* with x_t is also symmetrical.

To sum up, these results show that, unfortunately, the position of the effective surface cannot be predicted easily without solving the closure problem **Pb II**$_w$, except in two extreme cases. The first one is when the roughness are overlapping. Parameter δ^* will tend to one. The second one is when d_r is large enough to have δ^* close to zero. Besides these two limiting cases, it is required to solve the "*closure problem*".

4.2. Effective reactivity

In this part, we are particularly interested in the effect of chemical properties of the surface and flow characteristics on the effective reaction rate. The studied solid represents a composite. The chemical properties of the surface are limited to the reactivity of the matrix, k_m, and the fibers, k_f. For this analysis, two parameters are interesting: the mean value of the Damköhler number over the surface and the contrast between the reactivity of the fibers, and the matrix. The nomenclature used is

$$\widehat{Da} = \frac{Da_f A_f + Da_m A_m}{A_f + A_m} \quad \text{with } Da_j = \frac{k_j l_i}{D}, \tag{102}$$

$$r_k = \frac{k_m}{k_f} = \frac{Da_m}{Da_f}, \tag{103}$$

where A_f (resp. A_m) is the surface of the fibers (resp. matrix) in contact with the flow. Similarly, an averaged reaction rate can be defined, $\hat{k}$, and will be useful in the search of k_{eff} estimates

$$\hat{k} = \frac{k_f A_f + k_m A_m}{A_f + A_m}. \tag{104}$$

Flow conditions are characterized by the micro-scale Reynolds number and the Schmidt number defined by

$$Re_l = \frac{\rho \tau_h l^2}{\mu^2}, \tag{105}$$

$$Sc = \frac{\mu}{\rho D}. \tag{106}$$

The relationship between the global Reynolds number (defined in Eq. (4)) and the local one is

$$Re = O\left(\left(\frac{L}{l}\right)^2\right) Re_l. \tag{107}$$

High local Reynolds numbers imply that the model assumptions are no longer valid. High value of Re_l leads to $l/L^2 \gg Re$, which is equivalent to $l/L \gg Re$ as $l/L < 1$. In this case, terms neglected in Eq. (36) cannot be neglected anymore. Some special attention will be given to this fact in the analysis of the next results.

The dependence of the effective reaction rates k^0_{eff} and k^δ_{eff} on these different non-dimensional numbers is studied. Numerical simulations are done for the closure problem of variable a over elementary cells with a semi-ellipse roughness shape.

4.2.1. Effect of the surface chemical characteristics

Firstly, simulations are conducted for pure diffusion ($Re_l = 0$), avoiding possible effects of the flow properties. The impact of the mean Damköhler number and the reactivity contrast on k^0_{eff} are illustrated in Fig. 8. This figure shows two limits for the effective reaction rate k^0_{eff}. When the mean Damköhler number is small, the reactivity of the surface is low. As a consequence, the concentration will be nearly constant all over the cell. At the zeroth order, the closure variable is zero over the cell, giving the following expression for the effective reaction rate at Σ_0:

$$k^0_{\text{eff}} \approx \frac{1}{A_{0,i}} \int_\Sigma k \, dA. \tag{108}$$

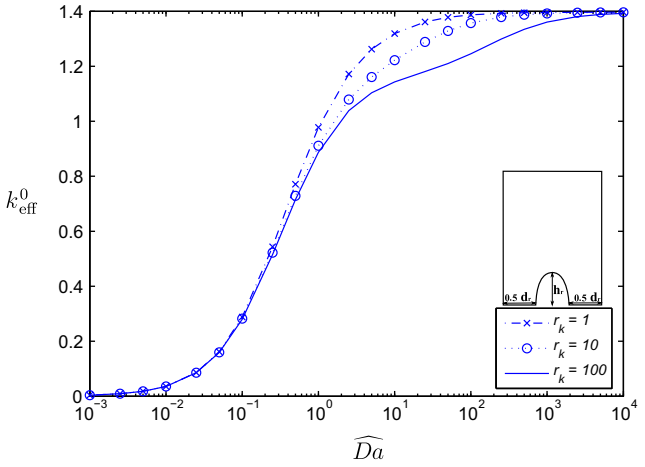

Fig. 8. Effective reaction rate, k^0_{eff} in function of the averaged Damköhler number, for different reactivity contrasts. Cell geometry: semi-ellipse shape with $h_r = 2.5e-6$ m and $(d_r/h_r) = 2$.

Therefore, k^0_{eff} can be estimated easily as

$$k^0_{\text{eff}} \approx \frac{\hat{k}A_\Sigma}{A_{0,i}} \quad \text{where } A_\Sigma = A_f + A_m. \tag{109}$$

This approximation is called k^0_{low}. One can note that this estimate do not depend on the position of Σ_0, contrarily to k^0_{eff}. This is the consequence of the previous zeroth-order approximation.

While this estimate of k^0_{eff} for low Damköhler number is different from the ratio D by w^0_x, the second effective reaction rate k^δ_{eff} (cf. Eq. (97)) has a defined limit. It can be written

$$k^\delta_{\text{eff}} \approx k^\delta_{\text{low}} = \frac{k^0_{\text{low}}}{1 - \frac{w^0_x}{D}k^0_{\text{low}}}. \tag{110}$$

As for k^δ_{eff}, k^δ_{low} depends on the position of Σ_{eff} through w^0_x. This new estimate does not exist when $k^0_{\text{low}} = D/w^0_x$, but this case cannot appear for low Damköhler number. Explanations can be found in Appendix B.

The second limit appears when the Damköhler number is high, the concentration close to the reactive surface is nearly equal to 0. In this case, the reaction rate k^0_{eff} also tends to a limit value which depends on the surface geometry.

Increasing the second parameter, the reactivity contrast decreases the value of k^0_{eff}. As a consequence, the limit for high Damköhler numbers appears for higher $\widehat{Da}$ values. Another point illustrated by this figure is that the contrast between the reactivities modifies the evolution of k^0_{eff} with $\widehat{Da}$. For a same $\widehat{Da}$, a higher r_k implies that the matrix has a stronger impact on the reaction at the surface. The fibers start to play a role in this exchange for higher Damköhler numbers when r_k increases. Nevertheless, the second limit for k^0_{eff} at high $\widehat{Da}$ does not depend on r_k.

Fig. 9 illustrates the evolution of the ratio k^0_{eff} over k^0_{low} with the mean Damköhler number. As expected, a good agreement is given between k^0_{eff} and its estimate for low $\widehat{Da}$. The graphs of Fig. 9 also show the fact that the contrast between the reactivities has nearly no impact on the ratio of k^0_{eff} over k^0_{low}. This result seems correct as for the case of low $\widehat{Da}$ at the zeroth order, the impact of matrix and the fibers is given by $\hat{k}$.

Tests with other geometries point out the dependence of the effective reaction rate with the surface shape (cf. Fig. 10). Fig. 10 shows how k^0_{eff} over k^0_{low} evaluates with the mean Damköhler number for different distance between asperities, d_r. Increasing this distance moves the curve forward.

These results were obtained in the purely diffusive case. In the following section, we analyze the impact of the velocity field on the effective reactivity.

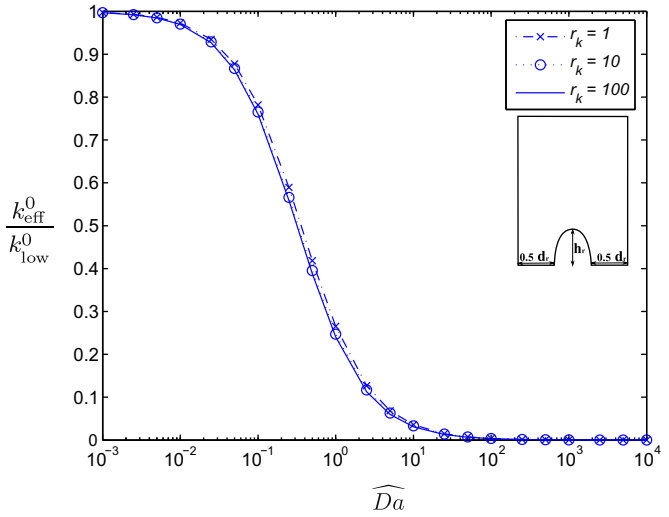

Fig. 9. Ratio k^0_{eff} over k^0_{low}, in function of the averaged Damköhler number, for different reactivity contrasts. Cell geometry: semi-ellipse shape with $h_r = 2.5e-6$ m and $(d_r/h_r) = 2$.

4.2.2. Effect of the flow properties

Previous work [23] on direct numerical simulation of laminar flow over reactive flat walls has shown that the competition between diffusion and advection (described by the *Pe* number) has poor impact on the consumed flux. In this study, the couple (Re_l, Sc) is chosen to parametrize the impact of flow characteristics on the effective reactivity.

In Fig. 11, the impact of this couple on the ratio of the effective reaction rate with convection over the one obtained in the purely diffusive case is illustrated by different graphs. *Sc* varies between 0.5 and 2, and *Re* between 1 and 5000. Results show that the Reynolds number has nearly no impact on the effective reaction rate, except for high values (Fig. 11) and confirm the trends obtained by direct simulation by [23]. This trend is also similar to the one observed for a reactive flat surface [24]. When the surface is flat, the transition between the diffusive regime and the convective regime appears for lower Reynolds numbers than for a rough surface. This is consistent with the fact that the asperities tend to decrease

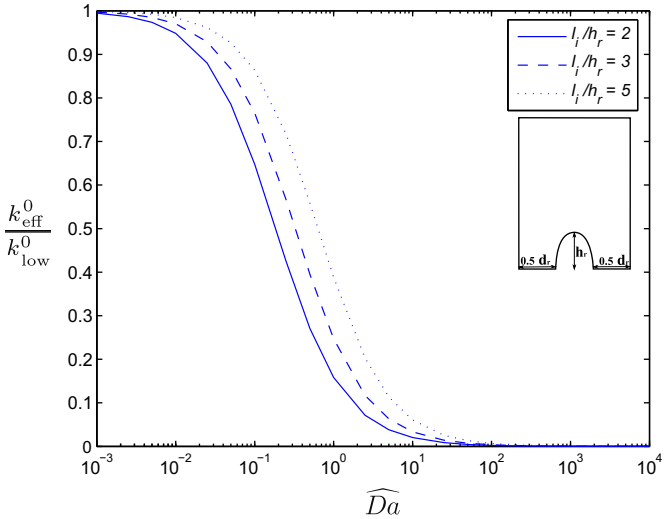

Fig. 10. Ratio k^0_{eff} over k^0_{low}, in function of the averaged Damköhler number, for different distances between asperities. Cell geometry: semi-ellipse shape with $h_r = 2.5e-6$ m.

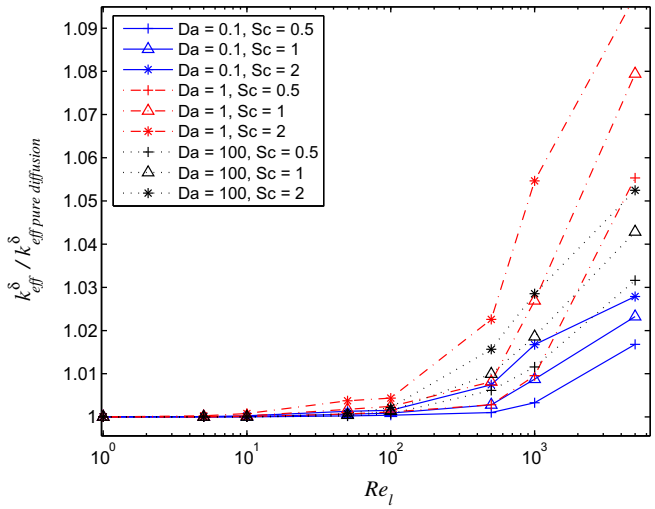

Fig. 11. Ratio between k^{δ}_{eff} with convection over k^{δ}_{eff} in the purely diffusive case, in function of the Reynolds number, for different Schmidt and Damköhler numbers.

rapidly the velocity in the surface neighborhood, thus increasing the diffusive regime as compared to the case of a flat surface.

For local Reynolds numbers inferior to 500 and Schmidt numbers lower than 2, k^{δ}_{eff} can be estimated by the value of k^{δ}_{eff} in pure diffusion with an error of less than 1%. For higher values of Re_l, the difference increases. At these high Reynolds numbers, the flow modifies significantly mass transport due to recirculations between asperities. As illustrated in Fig. 12, the total flux lines of variable a show that the flux is no longer normal to the surface, like for pure diffusion transfer. However, the variation of k^{δ}_{eff} at high Re_l is obtained for conditions that violate our initial assumption. Indeed, as it has been explained previously, these high values of Re_l imply really high values of the global Reynolds number and thus a turbulent boundary layer. In this case, the model detailed before is no more valid. Consequently, in a laminar boundary layer situation, it can be concluded that a good estimate of k^{δ}_{eff} is the value of k^{δ}_{eff} obtained for pure diffusion. The closure problems can be simplified accordingly.

The Schmidt number also affects k^{δ}_{eff}. As illustrated by the different graphs in Fig. 11, when the Schmidt number decreases the transition between the diffusive regime and the convective one is delayed. This result is expected as a decrease in Sc is equivalent to an increase in the molecular diffusion coefficient. Consequently, the transport by diffusion has more impact and extends the diffusive regime to higher Reynolds numbers. Nevertheless, in most applications, the effect of the Schmidt number on the effective reaction rate is not important and can be neglected.

To conclude, these results show that the closure problem **Pb II**$_a$ can be simplified by dropping the advective terms, as $k^{\delta}_{\text{eff}} \approx k^{\delta}_{\text{eff pure diffusion}}$. In addition, simulations in the pure diffusive regime point out limits for low and high Damköhler numbers. For low Da, k^{δ}_{eff} can be estimated quite easily with k^{δ}_{low}. In the next section, validation tests are conducted using this approximation of the effective reaction rate.

5. Numerical validation

Validation tests were done over the systems presented in Fig. 13. The rough surface is preceded by a flat and inert zone in order to have a developed boundary layer over the asperities. The reader should keep in mind that the first-order model described previously is only valid in these conditions (boundary layer flow and pseudo-periodicity). The flat zone remains unchanged after modelling, introducing a small step at the beginning of the asperities localization. Parameter δ gives the height of the step. This method differs from the one used in the work of Achdou et al., where the effective surface covers the flat surface of the wall and the rough one.

External boundary conditions are similar between the real system and the modelled one. Simulations over the detailed surface are done with a mesh of 34,369 elements with a minimum element quality of 0.49, compared to 15,440 elements with a minimum element quality of 0.52 for the simulations with the effective surface (cf. Fig. 14). In term of computational cost, simulations over the effective surface is two to four time more rapid than DNS over the detailed surface. The effective properties are obtained from the closure problems described previously.

At first, we compare the velocity fields obtained from the detailed simulation to the one with the effective surface. Figs. 15 and 16 show a good agreement between velocity fields. The results given with the effective surface are similar to the ones given over the rough wall, not taking into account the local fluctuations in the close surface neighborhood.

An interesting point is to prove that a specific treatment of the roughness effect is indeed necessary. Therefore, the velocity fields

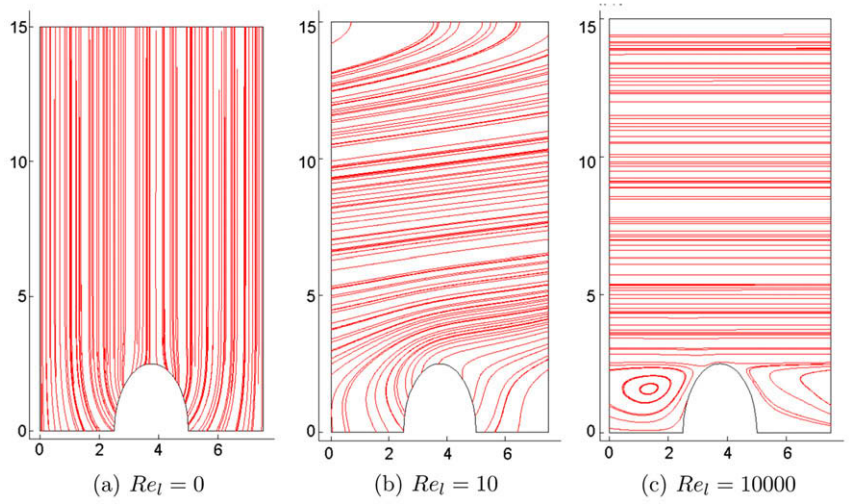

Fig. 12. Total flux lines of variable a with $Sc = 1$.

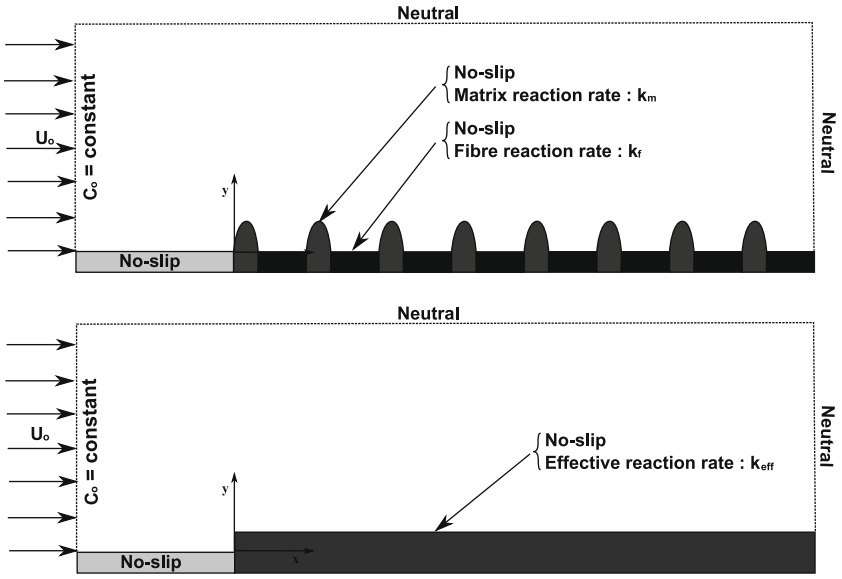

Fig. 13. Schematic representations of the different domains and boundary conditions used for validation tests. Upper figure: DNS, lower figure: first-order model.

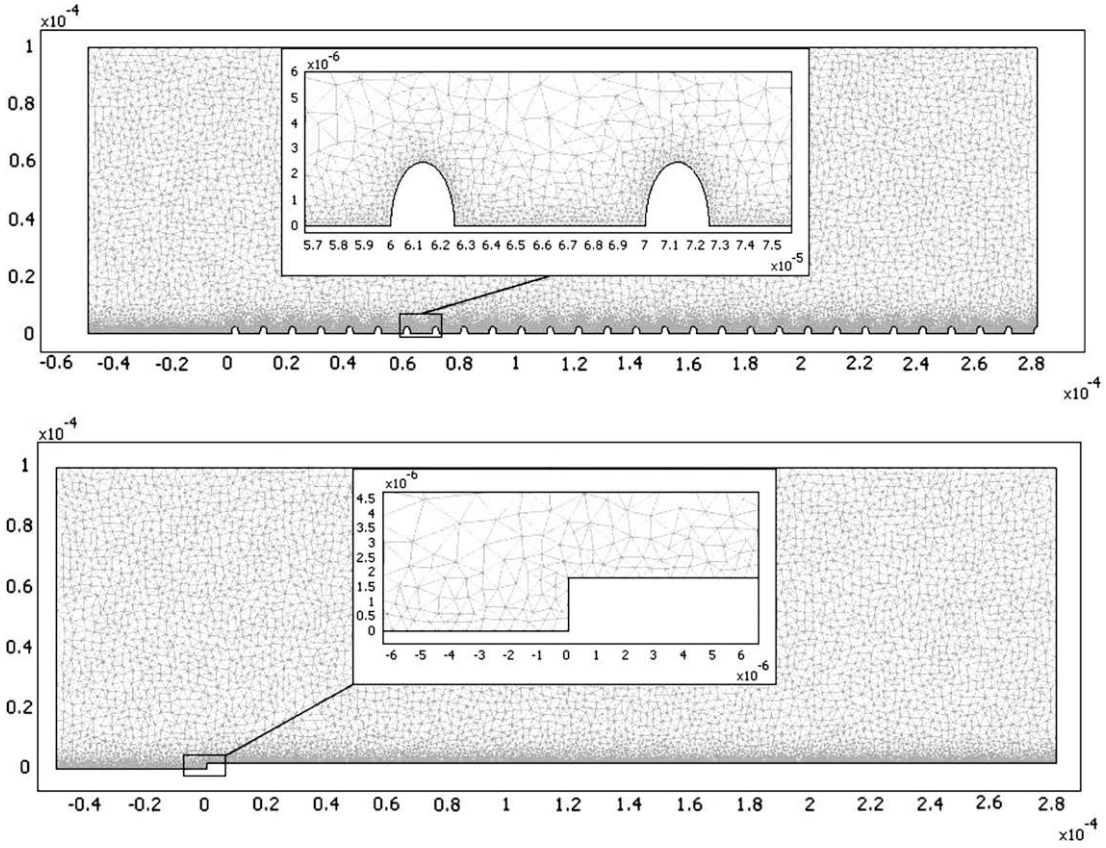

Fig. 14. Meshes used for DNS and simulation with the first-order model.

are also compared to the one obtained for a flat surface at $y = 0$. The velocity profiles are shown in Fig. 16. As expected the flat surface has a velocity profile very different of the one given by the rough surface. As a consequence, we may conclude that modelling taking into account roughness effect is indeed necessary. It is attractive to find that this model with an effective surface is a simple and good way to reproduce the actual velocity field on the whole domain.

Mass transfer is then added to this model as described before. The following results are obtained. Fig. 17 illustrates the good equivalence between the actual concentration field, i.e., the calculation with the rough surface, and the one given with the use of k_{eff}. Contours are well superposed except in the region before the step. Besides the comparison of the concentration field, the mass flux absorbed at the surface, J, and the total mass, N, are also studied. The errors observed on these two values are presented in Table

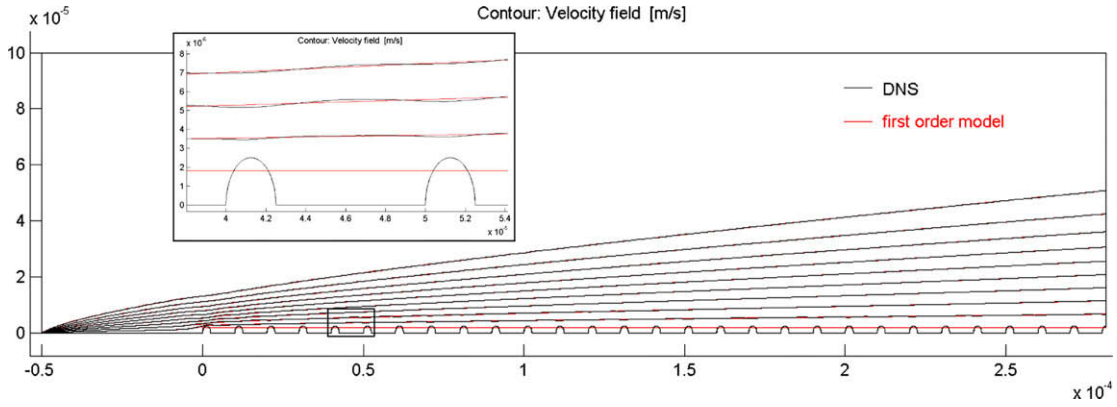

Fig. 15. Velocity field contours for the rough initial domain and the effective domain, for $Re = 10$.

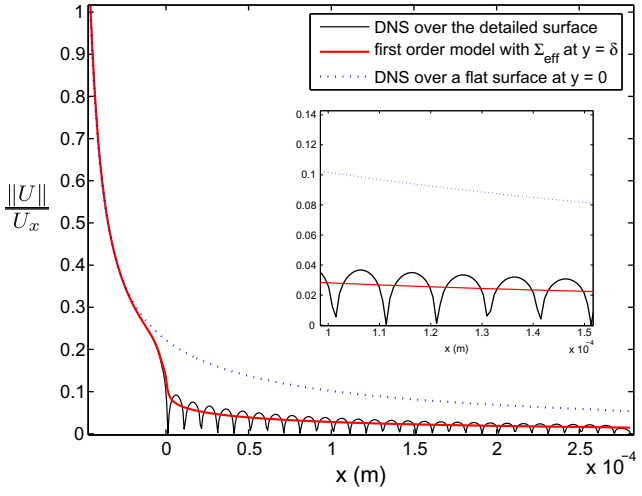

Fig. 16. Velocity profile at $y = h_r$ for a flow with $Re = 100$.

1. The effective model gives values similar to DNS values for J and N with less than 1.1% error. In the case of low Damköhler numbers ($\widehat{Da} = 0.001$), the approximation of the effective reaction rate is also tested. The results of Table 2 show that this estimate only introduce a slight difference on the error committed on J compared to the initial errors obtained with k^{δ}_{eff}. This difference on J-errors increases with the Damköhler number, e.g., $\widehat{Da} = 0.01$, $J_{\text{error}} < 4.5\%$ compared to the 1% obtained with the true effective reaction rate. Consequently, the estimate k^{δ}_{low} should be used carefully depending on the final expected error level.

Table 1
Error commited on the total mass and the mass flux exchanged over Σ.

Re (Re_l)	$\widehat{Da}$	r_k	Error on J	Error on N	r_k	Error on J	Error on N
10 (0.1)	0.01	1	0.00267	0.0108	10	0.00889	0.0111
10 (0.1)	1	1	0.00129	0.00303	10	0.0101	0.00988
10 (0.1)	10	1	0.000242	0.00160	10	0.00489	0.00536
100 (1)	0.01	1	0.00261	0.0109	10	0.00881	0.0110
100 (1)	1	1	0.000864	0.00327	10	0.00832	0.00470
100 (1)	10	1	0.00249	0.000065	10	0.00423	0.00190
1000 (10)	0.01	1	0.00342	0.0111	10	0.00968	0.0111
1000 (10)	1	1	0.00550	0.00533	10	0.00862	0.00549
1000 (10)	10	1	0.00463	0.00103	10	0.00953	0.00170

Both results are satisfactory and directly link to the fact that there is some errors committed on the mass transport close to the step. The modelling of mass transfer is not well adapted for the step region (i.e., $x \approx 0$) and the comparison of the concentration contours has already shown it. This was expected, since the model has been developed for pseudo-periodic asperities and the step zone does not match this condition. As a result, some errors are introduced. Nevertheless, the effective model does a very good job in predicting the velocity and the concentration fields.

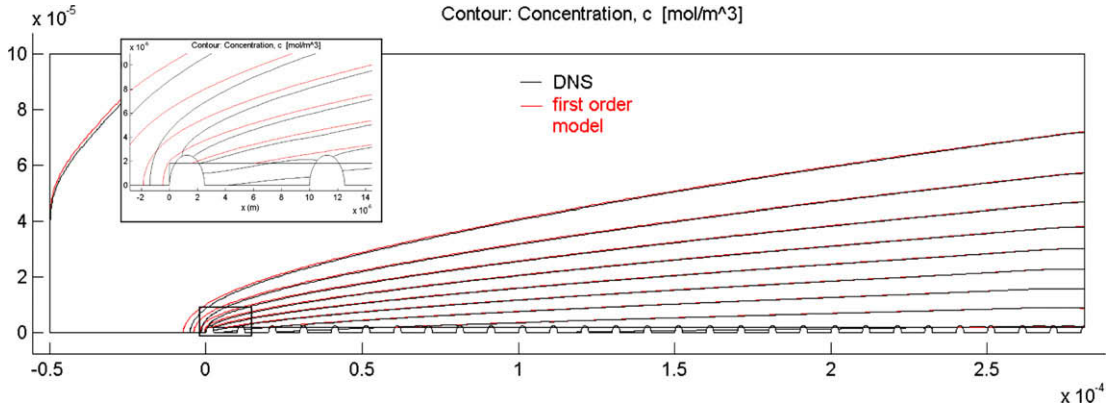

Fig. 17. Concentration field contours for the rough initial domain and the effective domain, for a flow entrance velocity of 10 m s^{-1}, $Da_f = 1$ and $r_k = 5$.

Table 2
Error commited on the total mass and the mass flux exchanged over Σ using the estimate of k_{eff} for low Da.

	Re (Re_l)	$\widehat{Da}$	r_k	Error on J	Error on N	r_k	Error on J	Error on N
k^{δ}_{eff}	10 (0.1)	0.001	1	0.00270	0.0112	10	0.00889	0.0112
k^{δ}_{low}	10 (0.1)	0.001	1	0.00599	0.0112	10	0.0123	0.0112
k^{δ}_{eff}	100 (1)	0.001	1	0.00265	0.0112	10	0.00884	0.0112
k^{δ}_{low}	100 (1)	0.001	1	0.00596	0.0112	10	0.0123	0.0112
k^{δ}_{eff}	1000 (10)	0.001	1	0.00338	0.0112	10	0.00972	0.0112
k^{δ}_{low}	1000 (10)	0.001	1	0.00670	0.0112	10	0.0132	0.0112

6. Conclusion

The objective of this work was to model momentum and mass transfer at the interface between a fluid phase and a rough, heterogeneous and reactive surface. This study was limited to the case of a laminar boundary layer flow over a pseudo-periodic rough surface, locus of a chemical reaction.

The technique to approximate the actual detailed solution was based on a domain decomposition idea involving a global domain and "roughness" unit cells. A first-order estimate of the link between the concentration and velocity fields in global domain and the unit cells was proposed under the form of mapping variables obeying two specific closure problems, one for each type of transfer. This allowed to propose a simplified model featuring a flat effective surface instead of the rough wall, on which new effective properties, in particular the effective reaction rates are entirely determined by the solution of the so-called closure problems. Their values were then analysed in function of the flow properties, as well as the surface geometrical and chemical characteristics. From this analysis, it has been concluded that assuming laminar boundary layer conditions, the flow has nearly no impact on the effective reaction rate. As a result, the closure problem for the concentration can be simplified to a pure diffusive one. In addition, two limiting cases were found for low and high Damköhler numbers. A finite limit for low $\widehat{Da}$ was determined and used as an estimate for the effective reaction rate, k^{δ}_{eff}, without major errors on the simulation results.

This model was tested through a comparison between DNS on the heterogeneous surface and simulations with the effective surface. Good agreements have been obtained between these different simulations. Velocity and concentration fields fitted very well, while some small differences were observed due to the entrance region effect, i.e., the beginning of the boundary layer. In future works, some special attention may be paid to the modelling of this step region.

As written in the introduction, this study is a part of a larger work on the ablation phenomenon of composite materials used in space technologies, even though it can be used in different engineering fields. This study can be extended to different transport mechanisms, more complex situations with, for instance, 3D patterns. In addition, the recession of the interface should be taken into account in the case of ablation.

Acknowledgements

The authors acknowledge Snecma Propulsion Solide (Safran group) for S. Veran Master thesis grant. They acknowledge Snecma Propulsion Solide associated to French Defense Procurement Agency (DGA) for Y. Aspa Ph.D. Thesis grant.

The advices given by Pr. Maruyama to S. Veran during a one-year stay in his laboratory, The Heat Transfer Control Laboratory at Tohoku University, are also gratefully acknowledged.

Appendix A. Mass loss

The Taylor development of the effective boundary condition at $y = 0$ to obtain the new boundary condition at $y = w^0_x$ conserves the flux exchange over Σ but not the total mass. This mass loss can be estimated. For an homogeneous and flat surface the evolution of the concentration towards the surface depends linearly with y:

$$C(y) = C_0|_{y=0}\left(1 - \frac{k^0_{\text{eff}} y}{D}\right), \tag{111}$$

in which y_s is the position of the surface. The "total mass" becomes

$$N_{y_s} = C_0|_{y=0}\left(y_s l_i - \frac{k^0_{\text{eff}} y_s^2 l_i}{2D}\right). \tag{112}$$

If we assume the existence of an effective surface which conserves N, the mass loss can be written

$$\widetilde{N} = C_0|_{y=0}\left(1 - \frac{k^0_{\text{eff}}(y_N + w^0_x)}{2D}\right)(y_N - w^0_x) l_i, \tag{113}$$

where y_N is the position of this effective surface conserving N.

Appendix B. k^{δ}_{eff} low Damköhler number limit

If the expression $k^0_{low} = D/w^0_x$ is developed, it gives

$$k_f A_f + k_m A_m = \frac{D}{w^0_x}. \tag{114}$$

Using the definition of the averaged Dhamkohler number (cf. Eq. (103)), it can be transformed into

$$\frac{\widehat{Da} D}{l_i}(A_f + A_m) = \frac{D}{w^0_x}. \tag{115}$$

The cell length, l_i, has the same order than $A_f + A_m$ giving this final approximation

$$\widehat{Da} \approx \frac{1}{w_x|_{y=0}}. \tag{116}$$

As $w_x|_{y=0} \ll 1$, this particular case can only happen when $\widehat{Da} \gg 1$, which is the opposite situation of the limit k^0_{low} which is valid for $\widehat{Da} \ll 1$. Therefore, the estimate of k^{δ}_{eff} as written in Eq. (110) is defined for any $\widehat{Da} \ll 1$.

References

[1] J. Nikuradse, Laws of flows in rough pipes, Technical Memorandum 1292, NACA, Washington, April 1937.
[2] J.A. Ochoa-Tapia, S. Whitaker, Heat transfer at the boundary between a porous medium and a homogeneous fluid, Int. J. Heat Mass Transfer 40 (11) (1997) 2691–2707.
[3] F.J. Valdés-Parada, J. Alberto Ochoa-Tapia, J. Alvarez-Ramirez, Diffusive mass transport in the fluid-porous medium inter-region: closure problem solution for the one-domain approach, Chem. Eng. Sci. 62 (2007) 6054–6068.
[4] G. Beavers, D. Joseph, Boundary conditions at a naturally permeable wall, J. Fluid Mech. 30 (1967) 197–207.
[5] J.A. Ochoa-Tapia, S. Whitaker, Momentum transfer at the boundary between a porous medium and a homogeneous fluid – I. Theoretical development, Int. J. Heat Mass Transfer 38 (14) (1995) 2635–2646.
[6] J.A. Ochoa-Tapia, S. Whitaker, Momentum transfer at the boundary between a porous medium and a homogeneous fluid – II. Comparison with experiment, Int. J. Heat Mass Transfer 38 (14) (1995) 2647–2655.

[7] B. Goyeau, D. Lhuillier, D. Gobin, M.G. Velarde, Momentum transport at a fluid-porous interface, Int. J. Heat Mass Transfer 46 (21) (2003) 4071–4081.
[8] M. Chandesris, D. Jamet, Boundary conditions at a fluid-porous interface: an a priori estimation of the stress jump coefficients, Int. J. Heat Mass Transfer 50 (17-18) (2007) 3422–3436.
[9] F.J. Valdés-Parada, B. Goyeau, J.A. Ochoa-Tapia, Jump momentum boundary condition at a fluid-porous dividing surface: derivation of the closure problem, Chem. Eng. Sci. 62 (15) (2007) 4025–4039.
[10] G. Duffa, G.L. Vignoles, J.-M. Goyhénèche, Y. Aspa, Ablation of carbon-based materials: investigation of roughness set-up from heterogeneous reactions, Int. J. Heat Mass Transfer 48 (16) (2005) 3387–3401.
[11] J. Lachaud, Y. Aspa, G. Vignoles, 3D modelling of thermochemical ablation in carbon-based materials: effect of anisotropy on surface roughness onset, in: Proc. of the 10th International Symposium on Materials in Space Environment (ISMSE 2006), ONERA,CNES, Collioure, France, 2006.
[12] J. Lachaud, Y. Aspa, G.L. Vignoles, Analytical modeling of the steady state ablation of 3D C/C composite, Int. J. Heat Mass Transfer 51 (9–10) (2008) 2614–2627.
[13] S. Whitaker, The Method of Volume Averaging, Kluwer Academic Publishers, Dordrecht, 1999.
[14] M. Chandesris, D. Jamet, Boundary conditions at a planar fluid-porous interface for a Poiseuille flow, Int. J. Heat Mass Transfer 49 (13-14) (2006) 2137–2150.
[15] F.J. Valdés-Parada, B. Goyeau, J. Alberto Ochoa-Tapia, Diffusive mass transfer between a microporous medium and an homogeneous fluid: jump boundary conditions, Chem. Eng. Sci. 61 (5) (2006) 1692–1704.
[16] B. Wood, M. Quintard, S. Whitaker, Jump conditions at non-uniform boundaries: the catalytic surface, Chem. Eng. Sci. 55 (22) (2000) 5231–5245.
[17] Y. Achdou, O. Pironneau, F. Valentin, Effective boundary conditions for laminar flows over periodic rough boundaries, J. Comput. Phys. 147 (1) (1998) 187–218.
[18] Y. Achdou, P. Le Tallec, F. Valentin, New wall laws for unsteady incompressible Navier–Stokes equations, in: European Congress on Computational Methods in Applied Sciences and Engineering, 2000.
[19] W. Jäger, A. Mikelić, On the roughness-induced effective boundary conditions for an incompressible viscous flow, J. Differ. Equations 170 (2001) 96–122.
[20] W. Jäger, A. Mikelić, Couette flows over a rough boundary and drag reduction, Commun. Math. Phys. 232 (2003) 429–455.
[21] A. Mikelić, V. Devigne, Ecoulement tangentiel sur une surface rugueuse et loi de Navier, Ann. Math. Blaise Pascal 9 (2) (2002) 313–327.
[22] Y. Achdou, P. Le Tallec, F. Valentin, O. Pironneau, Constructing wall laws with domain decomposition or asymptotic expansion techniques, Comput. Meth. Appl. Mech. Eng. 151 (1–2) (1998) 215–232.
[23] N.M. Juhasz, W.M. Deen, Effect of local Péclet number on mass transfer to a heterogeneous surface, Ind. Eng. Chem. Res. 30 (3) (1991) 556–562.
[24] Y. Aspa, Modélisation de l'Ablation des Composites C/C dans les Tuyères, Ph.D. Thesis, INPT, 2006.